High spin structure of ^{34}S and the proton-neutron coupling of intruder states

P. Mason,[1] N. Mărginean,[2,3] S. M. Lenzi,[1] M. Ionescu-Bujor,[3] F. Della Vedova,[1] D. R. Napoli,[2] T. Otsuka,[4,5] Y. Utsuno,[6] F. Nowacki,[7] M. Axiotis,[2,8] D. Bazzacco,[1] P. G. Bizzeti,[9] A. Bizzeti-Sona,[9] F. Brandolini,[1] M. A. Cardona,[10] G. de Angelis,[2] E. Farnea,[1] A. Gadea,[2] D. Hojman,[10] A. Iordachescu,[3] C. Kalfas,[8] Th. Kröll,[2] S. Lunardi,[1] T. Martínez,[2] C. M. Petrache,[11] B. Quintana,[1] R. V. Ribas,[12] C. Rossi Alvarez,[1] C. A. Ur,[1,3] R. Vlastou,[13] and S. Zilio[1]

[1]*Dipartimento di Fisica dell'Università and INFN, Sezione di Padova, Padova, Italy*
[2]*INFN-Laboratori Nazionali di Legnaro, Legnaro, Italy*
[3]*National Institute for Physics and Nuclear Engineering, Bucharest, Romania*
[4]*Department of Physics and Center for Nuclear Study, University of Tokyo, Hongo, Tokyo 113-0033, Japan*
[5]*RIKEN, Hirosawa, Wako-shi, Saitama 351-0198, Japan*
[6]*Japan Atomic Energy Research Institute, Tokai, Japan*
[7]*IReS, IN2P3-CNRS-Universitè Louis Pasteur, Strasbourg, France*
[8]*Institute of Nuclear Physics, NCSR Demokritos, Athens, Greece*
[9]*Dipartimento di Fisica dell'Università and INFN, Sezione di Firenze, Firenze, Italy*
[10]*Departamento de Física, CNEA, and CONICET, Buenos Aires, Argentina*
[11]*Dipartimento di Fisica dell'Università, Camerino, and INFN Sezione di Perugia, Italy*
[12]*Instituto de Fisica, Universidade de Sao Paolo, Brazil*
[13]*National Technological University of Athens, Athens, Greece*

(Received 18 October 2004; published 27 January 2005)

The nucleus ^{34}S has been studied up to relatively high spin ($I = 10\hbar$) and up to an excitation energy of 16.64 MeV. Data are compared with different shell model calculations where effective interactions involving two main shells, the *sd* and the *fp*, are used. For the first time in an $N \neq Z$ nucleus, it is observed that the promotion of an isoscalar ($T = 0$) proton-neutron pair to the *fp* shell becomes energetically favored at high spin.

DOI: 10.1103/PhysRevC.71.014316 PACS number(s): 21.10.−k, 21.60.Cs, 23.20.Lv, 27.30.+t

I. INTRODUCTION

Nuclei in the *sd* shell are a fundamental testing ground for many basic models of nuclear structure. Several interesting phenomena can be studied as a function of the angular momentu in this mass region such as clusterization, shape coexistence, proton-neutron interaction, and the interplay between collective and single-particle motion.

At high excitation energy, ^{32}S and neighboring nuclei are predicted to show superdeformed shapes [1], which could be associated to α clusterization [2]. In these nuclei, macroscopic-microscopic models, that is, SU(3), cluster model, and Hartree-Fock, can be compared to fully microscopic shell model calculations. The experimental information is, however, very scarce and many rigorous tests of nuclear models are necessary, especially in the high-spin region where excitations to the *fp* shell become important. A first attempt to cast light on this topic was a recent work on the nucleus ^{36}Ar [3]; in this nucleus, a superdeformed band ($\beta \sim 0.45$) was observed, whose origin was explained in terms of the excitation of two protons and two neutrons from the *sd* shell to the *fp* shell. Theoretical predictions of development of deformation at high spin in this mass region were also confirmed later by the observation of rotational bands in ^{38}Ar [4] and a superdeformed band in ^{40}Ca [5], where four protons and four neutrons are excited to the *fp* shell.

Nuclei near the $N = Z$ line are of great interest due to the symmetry displayed between proton and neutron degrees of freedom. This provides a unique way to study the effective proton-neutron (*pn*) interaction not only in the usual isovectorial ($T = 1$) coupling but also in states of isoscalar coupling ($T = 0$). Within the framework of the spherical shell model, this is due to protons and neutrons lying in the same shells, so that their orbits strongly overlap. Intensive efforts, both on the theoretical and the experimental side, have been spent over the last years on the investigation of the characteristics of the $T = 0$ pairing interaction and on its dependence on angular momentum and excitation energy. Although the relevance of the $T = 1$ pairing correlations is known to decrease rapidly with increasing angular momentum, the relative importance of $T = 0$ pairing is instead predicted to increase [6].

Recently, some relatively light $N \sim Z$ nuclei near ^{48}Cr were thoroughly studied. A peculiar feature of the nucleus ^{48}Cr and its neighbors is that the number of valence nucleons is small enough to allow exact full *fp* shell model calculations. Many of these nuclei display rotational bands that are well accounted for by shell model calculations in the full *fp* shell [7–9]. The existence of deformed structures has allowed to explore the dependence of *pn* correlations on the nuclear shape and the rotational frequency and effects due to the *pn* interaction were undoubtedly recognized in some of these nuclei [10].

In the $A \approx 30$–40 mass region, the low spin structure can be well reproduced by shell model calculations limited to the *sd* main shell with the USD residual interaction introduced by Wildenthal and Brown [11]. At high spins, where excitations of particles from the *sd* shell to the *fp* shell must absolutely be taken into account, shell model calculations bear still a considerable amount of uncertainty. In fact, a completely

reliable residual interaction, taking into account both the *sd* and the *fp* shell, has not yet been fully developed mainly due to the lack of data at high spin.

In this work, the high-spin structure of the nucleus ^{34}S ($N = 18$, $Z = 16$) is studied for the first time. Prior to our work very few states with $I \geqslant 5$ had been observed and for most of them no firm spin-parity assignment was given [12]. The new experimental results are reported in Sec. II and discussed in the framework of the shell model in Sec. III. Conclusions are given in Sec. IV.

II. EXPERIMENTAL RESULTS

Two experiments were performed to study high-spin states in ^{34}S through the reaction ^{24}Mg(^{16}O,$\alpha 2p$) at a bombarding energy of 70 MeV. In the first experiment the target consisted of a self-supporting foil of ^{24}Mg with a thickness of 400 μg/cm^2. For the second experiment a ^{24}Mg target, 750 μg/cm^2 thick, with a ^{197}Au backing of 15 mg/cm^2, was used to measure lifetimes with the Doppler shift attenuation method (DSAM). The beam was provided by the Tandem XTU accelerator of the Legnaro National Laboratory. Coincident γ rays were detected with the γ-spectrometer GASP, which consists of an array of 40 Compton-suppressed HPGe detectors and a multiplicity filter of 80 BGO scintillators. Events were collected when at least two HPGe detectors and one BGO scintillator fired in coincidence. Energy and efficiency calibration were performed with standard sources of ^{56}Co, ^{133}Ba, and ^{152}Eu. For the purposes of channel selection and kinematical reconstruction the 4π charged-particle detector ISIS (consisting of 40 ΔE-E Si telescopes) was also used.

For the thin target experiment a symmetric γ-γ matrix, concurrent with the detection of one α particle and two protons, was created for the construction of the ^{34}S level scheme. In this case the kinematical reconstruction of the recoil direction is absolutely necessary as the momentum of rather light recoil nuclei is heavily affected by particle evaporation; it improves the resolution by roughly 50% compared to a simple Doppler correction. To measure angular distributions of γ rays, the data were sorted into γ-γ matrices having on the first axis the detectors of the rings at 34°, 60°, 72°, 90°, 108°, 120°, and 146°, respectively, and on the second axis all the other detectors. The high statistics gathered by the GASP array gave us the possibility to measure the angular distribution of 16 transitions. Five of these transitions were previously unknown, and three, although observed in previous experiments, were not known in their multipolarity. When full angular distributions could not be determined, mainly because of low statistics, we resorted to the simpler method of ADO ratio (R_{ADO}) [13]. The ADO ratio is obtained as follows:

$$R_{\mathrm{ADO}} = \frac{I_{\gamma_1}(\text{at } 34^\circ \text{ gated by } \gamma_2)}{I_{\gamma_1}(\text{at } 90^\circ \text{ gated by } \gamma_2)}. \quad (1)$$

The gate on the γ_2 transition is set on the axis where all the detectors are added together. For stretched dipole transitions we obtained $R_{\mathrm{ADO}} \sim 0.75$ and $R_{\mathrm{ADO}} \sim 1.25$ for stretched quadrupole ones. In Table I we report the energy and intensity of the observed transitions, the angular distribution coefficients a_2 and a_4, the R_{ADO}, the deduced multipolarities, and the spin assignments.

The deduced level scheme of ^{34}S is shown in Fig. 1. There are 15 new levels placed at excitation energies higher than 9.4 MeV and with spin $I \geqslant 6$. A total of 38 new transitions has been observed in the decay of the excited ^{34}S. We note that, although ^{34}S gets particle unbound to alpha and proton decay at 7.92 and 10.88 MeV, respectively, higher excited states are bound due to the centrifugal barrier provided by the high spin. The spectrum shown in Figs. 2a and 2b has been obtained from the γ-γ-matrix after gating on the 1001, 1066, 2100, 2680, 2813, 3723, and 3814 keV transitions to put in evidence the transitions connecting high-spin states.

In Ref. [12] a 4^+ level at 6251.22 keV (decaying by two gammas of 1374 and 1562 keV) and a $(1,3)^-$ state at 6251.68 (decaying by two gammas of 572 and 1627 keV) were reported. In the present experiment all the four transitions are observed to deexcite the same level. This can be seen in Fig. 2c, where the spectrum in coincidence with the 1539 keV transition deexciting the 6^- level at 7790 keV [12] is shown. The new spin assignment for the 6251 keV level is 4^-, as the angular distribution of the 1539 keV transition indicates a quadrupole character and the measured short lifetime of the 6^- state, $\tau = 190$ fs (see below), is incompatible with an M2 transition.

Due to the low statistics obtained for the transitions between high-spin states, firm spin and parity assignments to some high-lying levels were not possible. Several non-yrast negative-parity states with $I \leqslant 6$ have also been observed in the present experiment. We report in Fig. 1 only those levels populated in the decay of the new high spin states.

The data registered in the gold-backed target experiment were sorted into seven asymmetric γ-γ coincidence matrices having on the first axis the detectors in rings at 34°, 60°, 72°, 90°, 108°, 120°, and 146°, respectively, and on the second axis all the other detectors. The 5^-, 5690 keV state in ^{34}S has a rather long lifetime of 53(3) ps [12], therefore the γ-rays deexciting it and the lower lying states are emitted from stopped nuclei. Experimental spectra were obtained from the asymmetric matrices by gating on these intense and narrow γ-lines. Doppler-broadened line shapes were observed for transitions deexciting the higher spin states. Level lifetimes were extracted from the line shapes using the code LINESHAPE [14]. The slowing down history of ^{34}S nuclei in the target and backing was simulated using Monte Carlo techniques and a statistical distribution was created for the projection of the recoil velocity with respect to the direction of the detected γ-ray. The shell-corrected Northcliffe and Schilling stopping powers [15] were used. Illustrative examples for experimental and calculated line shapes are shown in Fig. 3.

Lifetimes of about 250 fs were determined for the yrast positive-parity states 7^+, 9^+, and 10^+, whereas for the 8^+_1 state the lifetime was found to be much shorter, around 50 fs. For the 6^-_1 and 7^- states lifetimes of 190 and 122 fs, respectively, were measured, in rather good agreement with the previously reported values [12]. The assigned errors are rather large due to the uncertainties in the feeding processes and the short lifetimes. Using the experimental lifetimes and branching ratios, the reduced transition probabilities $B(M1)$ and $B(E2)$

TABLE I. Energy, intensity, angular distribution coefficients, ADO ratios, deduced multipolarity, and spin assignments for γ transitions in ^{34}S.

E_γ	I_γ^{rel}	A_2	A_4	R_{ADO}	Mult.	$I_i^\pi \rightarrow I_f^\pi$
356.3(6)	0.2(1)					$10_1^+ \rightarrow (9_2^+)$
572.0(1)	0.8(4)			0.72(13)	D	$4^- \rightarrow 3_2^-$
580.3(6)	0.6(3)			0.88(12)	D	$7^- \rightarrow 6_1^-$
942.3(5)	2.0(6)	−0.24(8)	−0.01(13)		D	$7^+ \rightarrow 6_2^-$
986.8(9)	0.8(4)					$8^- \rightarrow 6_4^-$
1001.6(5)	41.9(42)	−0.28(6)	0.02(15)	0.81(1)	D	$5^- \rightarrow 4^+$
1043.8(7)	0.7(4)					$6_4^- \rightarrow 7^-$
1055.4(8)	0.2(1)					$3_2^- \rightarrow 3_1^-$
1066.2(5)	34.9(35)	0.28(3)	−0.09(4)	1.35(3)	Q	$5^- \rightarrow 3^-$
1177.3(5)	22.5(23)					$2_2^+ \rightarrow 2_1^+$
1178(1)	1.0(5)					$7^+ \rightarrow 6_2^-$
1178(1)	0.5(3)					$(9_2^+) \rightarrow 8_3^+$
1180(1)	0.2(1)					$6_3^- \rightarrow 6_1^-$
1200.4(7)	3.2(7)			0.93(9)	D+Q	$10_1^+ \rightarrow 9_1^+$
1320.1(5)	26.6(27)	−0.29(7)	−0.01(20)	0.78(2)	D	$3^- \rightarrow 2^+$
1375.0(5)	2.8(6)					$4^- \rightarrow 3^+$
1384.5(14)	0.3(2)					$4^+ \rightarrow 2_2^+$
1408.6(9)	2.1(6)			0.8(1)	D	$7^+ \rightarrow 6^+$
1461.7(9)	3.7(8)			0.87(7)	D(+Q)	$8_1^+ \rightarrow 7^+$
1489.2(6)	0.7(4)					$9_1^+ \rightarrow 8_1^+$
1539.6(5)	5.0(10)	0.29(4)	−0.18(6)		Q	$6_1^- \rightarrow 4^-$
1541.5(5)	0.9(5)					$7^+ \rightarrow 7^-$
1562.5(5)	2.9(6)					$4^- \rightarrow 4^+$
1572.5(5)	3.2(7)					$3^+ \rightarrow 2^+$
1611.5(7)	0.6(3)					$(9_2^+) \rightarrow 8_2^+$
1626.7(5)	1.3(3)					$4^- \rightarrow 3^-$
1741.6(5)	1.2(3)					$9_1^+ \rightarrow 8^-$
1894.6(6)	1.5(3)					$8_3^+ \rightarrow 7^+$
1902.7(6)	0.9(5)					$\rightarrow 10_1^+$
1966.8(9)	2.6(6)			1.2(1)	Q	$10_1^+ \rightarrow 8_2^+$
2028.8(6)	3.3(7)					$8^- \rightarrow 7^-$
2099.6(8)	27.3(27)	−0.93(27)	0.38(69)	0.37(1)	D+Q	$6_1^- \rightarrow 5^-$
2122.9(6)	7.0(10)					$7^+ \rightarrow 6_1^-$
2127.5(6)	100	0.28(4)	−0.15(7)	1.23(3)	Q	$2_1^+ \rightarrow 0^+$
2147.2(6)	4.7(10)	0.49(6)	−0.29(9)	1.5(1)	Q	$8_1^+ \rightarrow 6^+$
2228.8(6)	9.5(11)			1.18(7)	Q	$9_1^+ \rightarrow 7^+$
2280.4(10)	4.7(10)	−0.11(8)	0.02(14)	0.74(4)	D	$8_1^+ \rightarrow 7^-$
2333.8(7)	1.2(5)					$(9_2^+) \rightarrow 8_1^+$
2375.4(7)	0.4(2)					$(3_2^-) \rightarrow 2_2^+$
2496.5(8)	12.3(12)	−0.31(9)	−0.14(22)	0.77(4)	D	$3^- \rightarrow 2_1^+$
2561.1(6)	67.5(65)	0.33(5)	−0.12(8)	1.24(4)	Q	$4^+ \rightarrow 2_1^+$
2608.6(6)	7.1(10)	0.45(3)	−0.23(5)	1.27(6)	Q	$8^- \rightarrow 6_1^-$
2680.5(6)	29.6(30)	0.40(2)	−0.19(2)	1.3(2)	Q	$7^- \rightarrow 5^-$
2688.4(8)	0.7(4)					$\rightarrow (10_2^+)$
2749.6(6)	3.6(8)					$3^+ \rightarrow 2_1^+$
2768.9(9)	0.7(4)					$(10_3^+) \rightarrow 8_3^+$
2812.7(9)	7.7(14)	−0.41(21)	−0.03(33)	0.69(5)	D	$6^+ \rightarrow 5^-$
2920.1(10)	0.5(3)					$(9^-) \rightarrow 8^-$
3002.8(6)	4.1(8)	−0.36(24)	−0.03(33)	0.65(5)	D	$8_2^+ \rightarrow 7^-$
3044.1(6)	3.1(7)			1.06(8)	D+Q	$6_2^- \rightarrow 5^-$
3280.0(6)	3.5(7)					$6_3^- \rightarrow 5^-$
3304.6(7)	17.8(18)	0.34(8)	−0.14(11)		Q	$2_2^+ \rightarrow 0^+$
3308.8(8)	3.0(6)					$(10_2^+) \rightarrow 8_1^+$
3436.1(6)	1.5(6)			0.67(8)	D	$8_3^+ \rightarrow 7^-$
3551.2(6)	0.6(3)					$3_2^- \rightarrow 2_1^+$

TABLE I. (*Continued*.)

E_γ	$I_\gamma^{\rm rel}$	A_2	A_4	$R_{\rm ADO}$	Mult.	$I_i^\pi \rightarrow I_f^\pi$
3562.7(6)	1.2(5)					$5^- \rightarrow 2_1^+$
3722.6(6)	3.3(7)			0.91(9)	D+Q	$6_4^- \rightarrow 5^-$
3813.6(7)	3.9(8)					$6^+ \rightarrow 4^+$
4880.8(16)	1.8(5)					$\rightarrow 8^-$
4949.3(18)	1.9(4)					$(9^-) \rightarrow 7^-$

have been derived. A pure $M1$ character was assumed for the 580-, 1200-, and 1409-keV $\Delta I = 1$ transitions, as the corresponding $R_{\rm ADO}$ values indicate negligible small mixing. For the 2100-keV $6_1^- \rightarrow 5^-$ transition a rather large mixing coefficient $\delta = -1.8(1)$ has been derived on the basis of the angular distribution coefficients (see Table I), in very good agreement with previous data [12]. For this $\Delta I = 1$ transition, both $B(M1)$ and $B(E2)$ values could be deduced. The experimental results concerning the lifetimes and the reduced transition probabilities are presented in Table II.

III. DISCUSSION

The low-spin structure of *sd* shell nuclei can be reproduced with good accuracy by means of the spherical shell model using the USD residual interaction for the *sd* shell model space [11]. Nevertheless, to cope with the high-spin spectroscopy of these nuclei, one has to consider a larger valence space as excitations involving one or more particles in the *fp* shell become important. This implies not only huge matrices to diagonalize but also an effective interaction that takes into account two main shells. In the past few years several theoretical efforts have focused on the explanation or prediction of the structure of neutron-rich isotopes in this mass region. Intruder states of those calculations actually mean that valence protons were still confined practically to the *sd* shell, whereas neutrons were excited from the *sd* to the *pf* shell. This implies that the proton-neutron correlation in the *pf* shell did not come into the game.

In the present work we report the outcomes of three shell model calculations using different interactions and model spaces. We refer first to the positive parity states. A first calculation (*sd*) was performed with the code ANTOINE [16] in the *sd* shell model space using the USD residual interaction [11]. In this valence space the maximum possible angular momentum is $I^\pi = 10^+$. The calculated yrast levels are compared with data in Fig. 4. Although the low spin states are

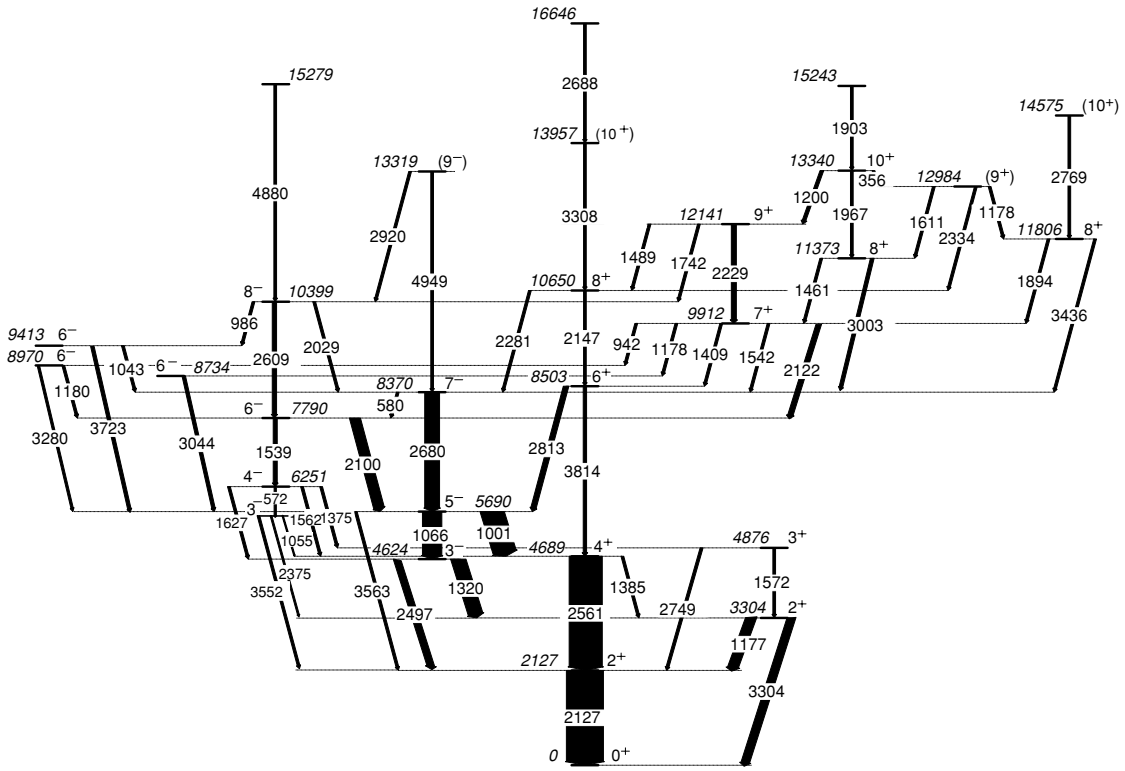

FIG. 1. Level scheme of ^{34}S as observed in the present experiment.

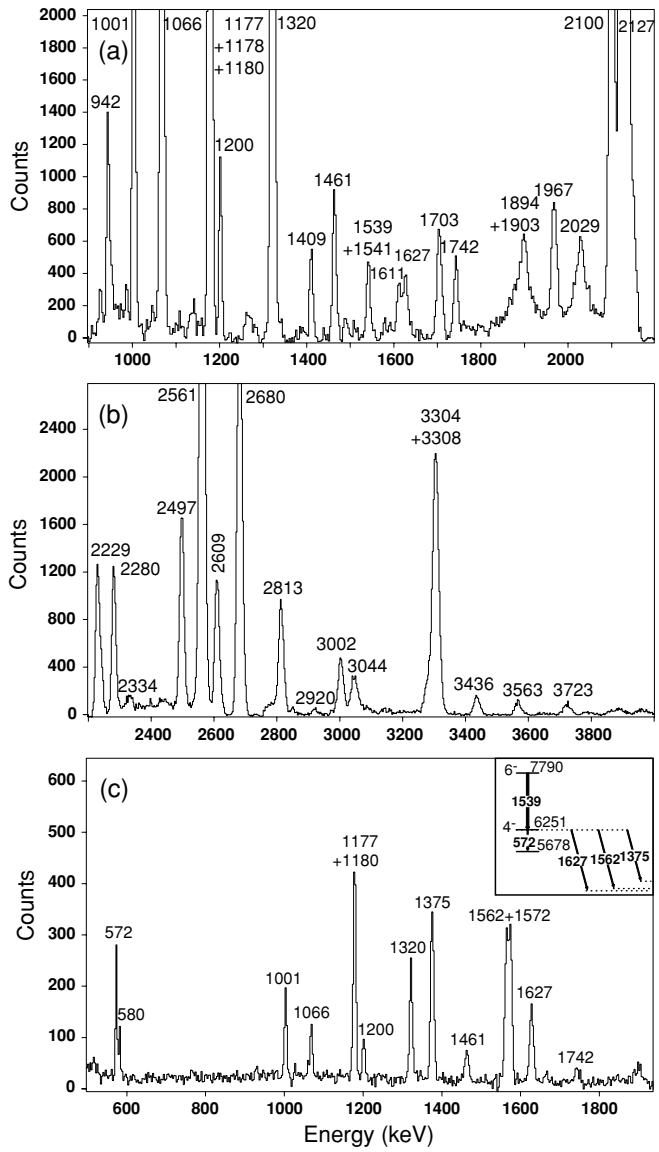

FIG. 2. (a)–(b) Coincidence spectrum with gates set on the 1001, 1066, 2100, 2680, 2813, 3723, and 3814 keV transitions in ^{34}S; (c) spectrum in coincidence with the 1539 keV ($6^- \rightarrow 4^-$) transition.

well reproduced, states with $I^\pi > 6^+$ are predicted too high in energy. To construct positive parity states with excitations in the *fp* shell, at least two nucleons have to be promoted from the *sd* shell.

An exact diagonalization for ^{34}S is feasible with the code ANTOINE in the $s_{1/2}d_{3/2}f_{7/2}p_{3/2}$ shell model space. The truncated space assumes a ^{28}Si inert core and, therefore, no excitations from the $d_{5/2}$ orbit are considered. The effective interaction, called *sdfp* [17], has been constructed by using the USD and KB3 [18] interactions for the *sd* and *fp* shells, respectively, combined with the cross-shell interaction whose matrix elements are calculated using the G matrix of Kahanna, Lee and Scott [19]. The results compare well with data for the high spin states (Fig. 4), whereas, for low spins the closure of the $d_{5/2}$ orbit has a strong impact.

The constraint of a closed ^{28}Si core can be released in a calculation done with the Monte Carlo shell model (MCSM) [20]. The valence space in this case is $d_{5/2}s_{1/2}d_{3/2}f_{7/2}p_{3/2}$ and the interaction consists of three parts. For the *sd* shell the USD interaction is used, and the Kuo-Brown interaction [21] is adopted for the *fp* part, whereas for the cross-shell part, the interaction of Ref. [22], based on the Millener-Kurath interaction [23], is used. On top of the combination of these interactions, small but rather important corrections have been made on the USD part to correct the neutron dripline of oxygen isotopes. This interaction has been introduced in [24], whereas it was called SDPF-M later [25]. As shown in Fig. 4, apart from the $I^\pi = 7^+$ state, which is predicted to be too high in energy, the agreement of MCSM results with the data is good.

To have a deeper insight on the calculations we have extracted the occupation numbers of protons and neutrons in the $f_{7/2}p_{3/2}$ orbits. The results for the positive parity states are summarized in upper part of Table III. The excitation of nucleons to the *fp* shell becomes important at $J = 6^+$, where both calculations indicate the promotion of two neutrons. In the case of the 7^+ state, the excitation of a *pn* pair starts to compete with that of two neutrons in *sdfp* calculations that reproduce well its excitation energy. Conversely, it is not well reproduced by MCSM calculations that predict for the 7^+ state a pure *2n* excitation to the *fp* shell. The disagreement for the SDPF-M interaction used in MCSM calculations is considered to be mainly due to certain properties of the Kuo-Brown *pf* shell interaction [21] in the $T = 0$ channel. This problem has been untouched in the SDPF-M interaction for simplicity, because it has no significant influence on excitations or mixings of two neutrons between the *sd* and *pf* shells. The problem, however, arises when $T = 0$ pairs of nucleons in the *pf* shell play some explicit role. The present experiment is indeed such a case for the first time and provides precious information for the improvement needed in this respect.

A remarkable feature is that the configuration with a proton-neutron pair in the *fp* shell is dominant in the 8_2^+ and 9_1^+ states. This fact merits a deeper investigation. For this purpose we have calculated the expectation value of the T^2 operator in the *sd* and *fp* valence spaces separately. These values can tell us, in particular, how the proton and the neutron are coupled in the *fp* space. It could become energetically favored to promote a proton and a neutron coupled to the maximum spin in the *fp* shell ($I = 7$) when they are in a $T = 0$ coupling (*pn*), instead of two identical nucleons coupled to $T = 1$ with maximum spin $I = 6$ (*2p* or *2n*). This seems to happen for the 9_1^+ state where the expectation value of the T^2_{fp} operator in the *fp* shell vanishes, whereas in the *sd* space it is maximum $[T(T+1)_{sd} \simeq 2]$. For this state, the expectation value of the I^2_{fp} operator indicates a $I = 7$ *pn* coupling. For the yrare 9_2^+ state, SDPF-M calculations predict the excitation of a neutron pair to the *fp* shell, whereas the *sdfp* shell model gives a mixed (*2n*/*pn*) configuration. The decay pattern is in better agreement with the latter proposed configuration.

The two 10^+ states have very different configurations as results from the calculations. In fact, *sdfp* calculations predict that the yrast 10^+ corresponds to the promotion of a proton-neutron pair (*pn*) to the *fp* shell, whereas the

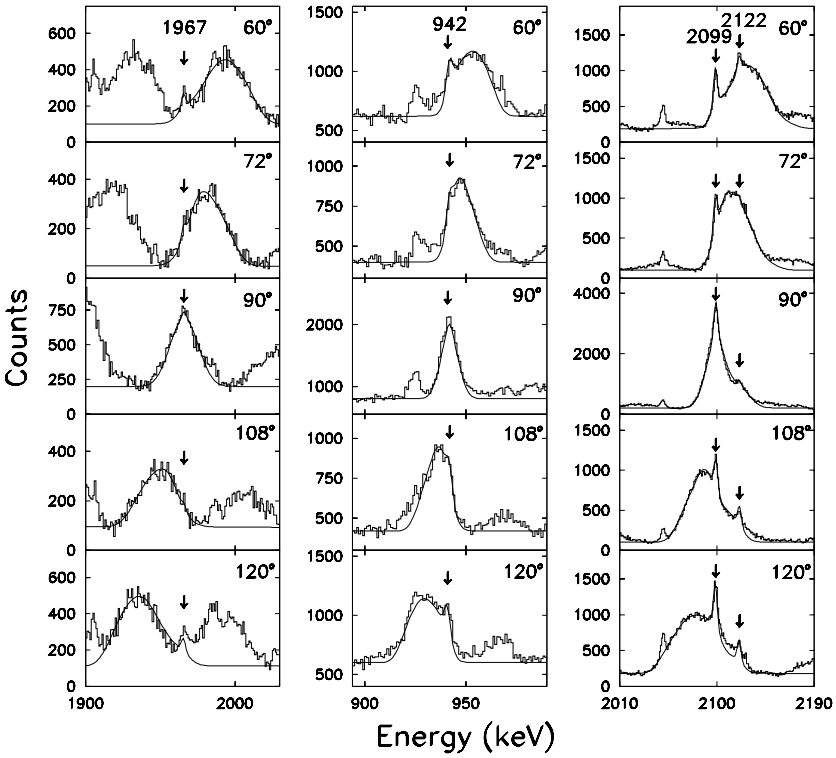

FIG. 3. Experimental and fitted line shapes in the measurement with the gold-backed target, for the 1967-, 942-, 2122-, and 2100-keV transitions deexciting the states at 13340, 9912, and 7790 keV, respectively.

yrare one is constructed by promoting two neutrons ($2n$). This is in agreement with the experimental decay pattern and the transition probabilities (see below). The SDPF-M calculations give the first and second 10^+ states apart from each other by about 1 MeV. As discussed later, these correspond respectively to the *second* and *first* 10^+ states observed experimentally.

The experimental reduced transition probabilities $B(M1)$ and $B(E2)$ obtained in the present work for high-spin states in ^{34}S are compared in Table II with the results of *sdfp* and SDPF-M calculations. There is an overall agreement between the experimental and theoretical values. For the transitions involving the 7^+ and 10^+ states for which, as discussed above, SDPF-M does not give a good description, the agreement is not that good. As shown in Table II, the inversion of the 10^+ SDPF-M states is sustained by the transition probabilities: the data for the decay of the 10^+_1 state are in better agreement with SDPF-M values corresponding to the calculated 10^+_2 state: $B(M1 : 10^+_2 \rightarrow 9^+_1) = 0.084\mu^2_N$ and $B(E2 : 10^+_2 \rightarrow 8^+_2) = 16\ e^2\,fm^4$.

From the above discussion we can deduce that at high spin, the promotion of a proton-neutron pair—coupled to $I = 7, T = 0$—to the *fp* shell becomes favored with respect to the promotion of a pair of neutrons. To our knowledge, this is the first time where this type of coupling is observed in an $N \neq Z$ nucleus.

TABLE II. Experimental lifetimes and reduced transition probabilities $B(M1)$ and $B(E2)$ obtained in the present work compared to the shell model results for ^{34}S. In deriving the theoretical $B(M1)$ values, free nucleon g factors have been used. The *sdfp* $B(E2)$ values have been calculated with effective electric charges $e^{\text{eff}}_\nu = 0.5e$ and $e^{\text{eff}}_\pi = 1.5e$, whereas for the SDPF-M $B(E2)'s$, $e^{\text{eff}}_\nu = 0.5e$ and $e^{\text{eff}}_\pi = 1.3e$ were used. The numbers in brackets for SDPF-M calculations correspond to the results for the 10^+_2 state. Details are explained in the text.

						$B(M1)(\mu^2_N)$			$B(E2)(e^2 fm^4)$		
I^π	$E^{\text{exp}}_{\text{lev}}$ (keV)	τ_{exp} (fs)	I^π_f	E^{exp}_γ (keV)	BR_{exp} %	exp	*sdfp*	SDPF-M	exp	*sdfp*	SDPF-M
7^+	9912	265(55)	6^+	1409	16(5)	0.012(5)	0.008	0.095			
8^+_1	10650	50(25)	6^+	2147	50(12)				179(97)	53	91
9^+_1	12141	250(50)	7^+	2229	83(11)				49(12)	24	0.16
10^+_1	13340	260(40)	9^+_1	1200	54(12)	0.068(18)	0.129	0.011(0.084)			
			8^+_2	1967	44(11)				47(14)	24	2(16)
6^-_1	7790	190(50)	5^-	2100	80(9)	0.006(2)	0.002	0.000	64(25)	12	38
			4^-	1539	15(4)				77(28)	29	35
7^-	8370	122(40)	6^-_1	580	2(1)	0.054(32)	0.037	0.044			
			5^-	2680	98(10)				47(16)	35	32

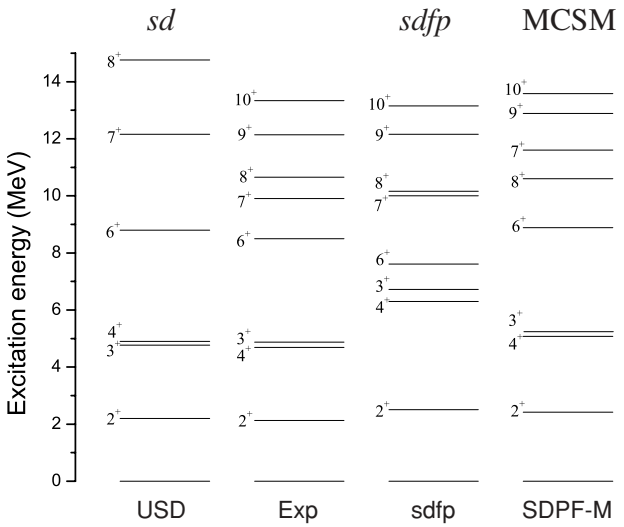

FIG. 4. Experimental yrast positive parity levels of ^{34}S compared to different shell model calculations (see text for details).

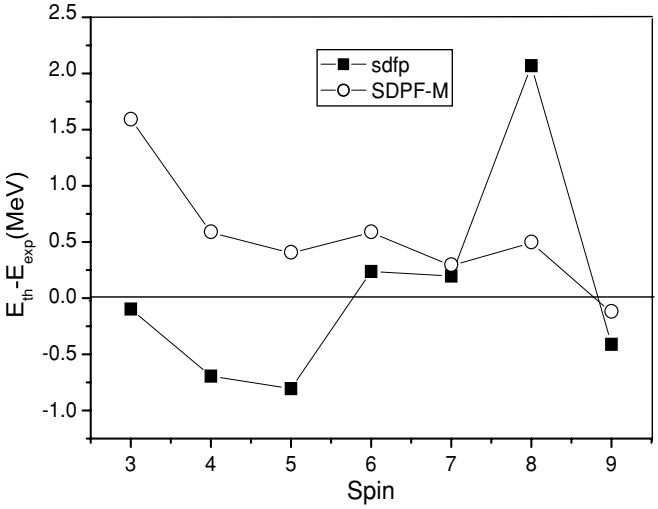

FIG. 5. Shell model minus experimental yrast negative parity levels of ^{34}S (see text for details).

Yrast negative parity states are well described by the two calculations (see lower parts of Tables II and III). These states are mainly constructed by promoting a neutron to the *fp* shell. For the 8^- state *sdfp* calculations give an important contribution of three particles in the *fp* shell. The constraint of keeping the $d_{5/2}$ shell closed in these calculations may be the responsible for the predicted too high energy. For the 9^- state the two calculations give different configurations. In the framework of the *sdfp* space, the 9^- state is formed with at least three particles in the *fp* shell. In the SDPF-M results, the contribution of excitations from the $d_{5/2}$ becomes very important. Both mechanisms of constructing a 9^- state involve a high energy transition, consistent with data.

The difference between the calculated and experimental energies for negative parity states is reported as a function of the angular momentum in Fig. 5. For low spin, where one nucleon is promoted to the *fp* shell, both calculations differ by $\sim$1 MeV. This could reflect a larger $f_{7/2} - d_{3/2}$ gap in ^{34}S for the SDPF-M interaction than for the *sdfp*. In this way, the

TABLE III. Experimental yrast and yrare level energies compared to the results of the *sdfp* and SDPF-M calculations for ^{34}S. Calculated neutron (*n fp*) and proton (*p fp*) occupation numbers in the *fp* shell are given for each state.

	Exp	sdfp			SDPF-M		
I^π	E (MeV)	E (MeV)	*n fp*	*p fp*	E (MeV)	*n fp*	*p fp*
0^+	0	0	0.47	0.13	0	0.26	0.12
2^+	2.13	2.51	0.22	0.30	2.50	0.20	0.12
3^+	4.87	6.72	0.35	0.12	5.15	0.22	0.12
4^+	4.69	6.31	0.40	0.18	5.08	0.21	0.11
6^+	8.50	7.61	2.00	0.2	8.89	1.99	0.11
7^+	9.91	10.03	1.78	0.45	11.63	1.97	0.08
8^+_1	10.65	10.16	2.00	0.2	10.68	1.99	0.08
8^+_2	11.37	11.30	1.27	0.91	12.89	1.39	0.67
9^+_1	12.14	12.16	1.32	0.87	12.88	1.08	0.96
9^+_2	12.98	13.12	1.47	0.78	13.65	1.97	0.02
10^+_1	13.34	13.15	1.24	0.93	13.58	1.98	0.07
10^+_2	13.95	14.30	1.91	0.24	14.57	1.07	0.98
3^-_1	4.62	4.52	1.02	0.22	6.19	0.98	0.17
4^-	6.25	5.56	1.10	0.16	6.83	1.07	0.09
5^-	5.69	4.89	1.08	0.14	6.09	1.02	0.09
6^-	7.79	8.02	1.13	0.16	8.37	1.05	0.10
7^-	8.37	8.56	1.12	0.09	8.66	1.04	0.07
8^-	10.40	12.44	1.30	0.28	10.89	1.02	0.06
9^-	13.32	12.91	2.68	0.60	13.20	1.04	0.06

study of nonnatural parity states becomes an interesting tool to "measure" the gap and improve interactions involving two main shells.

The 3^- state is predicted high in energy with the SDPF-M interaction, and the deviation is much larger than other negative-parity yrast states. This may be due to the fact that the 3^- state is an octupole vibrational state requiring the full *pf* shell orbits for its description. The other negative-parity states are more likely single-particle $1p-1h$ states, sensitive mainly to the shell gap energy. It is important to note that the major hole orbit changes with increasing spin, being the $d_{5/2}$ at $J=9$ in MCSM calculations.

IV. CONCLUSIONS

The nucleus ^{34}S has been studied for the first time in its high-spin region in fusion-evaporation reactions between heavy ions. The high sensitivity of the experimental setup allowed us to extend the positive-parity yrast states up to 10^+ (13.34 MeV) and the negative-parity ones up to 9^- (13.32 MeV). Levels of even higher excitation energy were identified (up to 16.64 MeV), although it was not possible to assign spin or parity to them. A total of 15 new levels and 38 new transitions have been observed. Using the DSAM, the lifetimes of several high spin states have been determined.

From the theoretical point of view, high-spin states in the nucleus ^{34}S represent a valid test for cross-shell residual interactions. The comparison between the outcomes of shell model calculations and the experimental data suggests that the adopted interactions, although conceived for the description of neutron-rich nuclei, work fairly well also along the stability valley, although there is still room for improvement. Calculations provide additional information about the kind, number, and isospin coupling of particles that are promoted to the *fp* shell. Structures with four particles in the *fp* shell, which should give rise to a superdeformed band, have not been identified in the present experiment.

The hint at the competition between isovector and isoscalar couplings in the intruder orbits for high-spin states of ^{34}S opens a new perspective in the study of this phenomenon also in $N \neq Z$ nuclei.

ACKNOWLEDGMENTS

This work has been partly supported by the TMR European Contract HPRI-CT-1999-00083, by a Grant-in-Aid for Specially Promoted Research (13002001) from the MEXT (Japan), and by the RIKEN-CNS collaboration project on large-scale nuclear structure calculations.

[1] H. Molique, J. Dobaczewski, and J. Dudek, Phys. Rev. C **61**, 044304 (2000).
[2] J. Zhang and W. D. M. Rae, Nucl. Phys. **A564**, 252 (1993).
[3] C. E. Svensson *et al.*, Phys. Rev. Lett. **85**, 2693 (2000).
[4] D. Rudolph *et al.*, Phys. Rev. C **65**, 034305 (2002).
[5] E. Ideguchi *et al.*, Phys. Rev. Lett. **87**, 222501 (2001).
[6] W. Satula and R. Wyss, Nucl. Phys. **A676**, 120 (2000).
[7] E. Caurier, J. L. Egido, G. Martínez-Pinedo, A. Poves, J. Retamosa, L. M. Robledo, and A. P. Zuker, Phys. Rev. Lett. **75**, 2466 (1995).
[8] S. M. Lenzi *et al.*, Z. Phys. A **354**, 117 (1996).
[9] F. Brandolini *et al.*, Nucl. Phys. **A642**, 387 (1998).
[10] A. Poves, J. Phys. G **25**, 589 (1999).
[11] B. A. Brown and B. H. Wildenthal, Ann. Rev. Nucl. Part. Sci. **38**, 29 (1988).
[12] P. M. Endt, Nucl. Phys. **A633**, 1 (1998).
[13] M. Piiparinen *et al.*, Nucl. Phys. **A605**, 191 (1996).
[14] J. C. Wells and N. R. Johnson, Report No. ORNL-6689, 1991, p. 44.
[15] L. C. Northcliffe and R. F. Schilling, Nucl. Data Tables A **7**, 233 (1970).
[16] E. Caurier, shell model code ANTOINE, Ires, Strasbourg, 1989–2004; E. Caurier and F. Nowacki, Acta. Phys. Pol. **30**, 705 (1999).
[17] E. Caurier, K. Langanke, G. Martínez-Pinedo, F. Nowacki, and P. Vogel, Phys. Lett. **B522**, 240 (2001).
[18] A. Poves and A. P. Zuker, Phys. Rep. **70**, 4 (1981).
[19] S. Kahana, H. C. Lee, and C. K. Scott, Phys. Rev. **180**, 956 (1969).
[20] T. Otsuka, M. Honma, and T. Mizusaki, Phys. Rev. Lett. **81**, 1588 (1998).
[21] T. T. S. Kuo and G. E. Brown, Nucl. Phys. **A114**, 241 (1968).
[22] F. K. Warburton *et al.*, Phys. Rev. C **34**, 1031 (1986).
[23] D. J. Millener and D. Kurath, Nucl. Phys. **A255**, 315 (1975).
[24] Y. Utsuno, T. Otsuka, T. Mizusaki, and M. Honma, Phys. Rev. C **60**, 054315 (1999).
[25] Y. Utsuno, T. Otsuka, T. Glasmacher, T. Mizusaki, and M. Honma, Phys. Rev. C **70**, 044307 (2004).